Optimization And Biodegradability Of High-Strength Polyamide Fiber Process

Yapei Wang

Pingdingshan Polytechnic College, Pingdingshan 467001, China

Corresponding author. E-mail: peiya666@163.com

Received: Feb. 08, 2025; Accepted: Jun. 05, 2025

High-strength polyamide fiber is a commonly used polymer material, but its degradation is difficult and has obvious impacts on the environment. Therefore, the study proposes to optimize the production process of high-strength polyamide fibers by combining composite titanium dioxide with biodegradable additives. The results showed that after optimizing the production process, the weight loss of the sample after 125 days of soil degradation treatment could reach 18.583%. The experimental samples began to degrade at 400°C, and the residual mass of all samples was less than 2%. After adding composite modified titanium dioxide and biodegradable additives, the tensile strength slightly decreased, and the toughness also slightly decreased. After soil degradation treatment, the macromolecular chains of the optimized sample underwent significant changes, and the number of high-polymer molecules was decomposed into various short chain macromolecular polymers. After optimizing the production process, the biodegradation level of high-strength polyamide fibers significantly increased, and their natural degradation rate significantly accelerated. The mechanical properties of high-strength polyamide fibers only slightly decreased. The optimized production process for high-strength polyamide fibers can effectively improve the degradation level of such products and increase their application scope.

Keywords: Polyamide fiber; Biodegradation; Titanium dioxide; Full dull; Infrared spectrum

http://dx.doi.org/10.6180/jase.202604_29(4).0004

1. Introduction

Polyamide fiber, commonly known as nylon, is a general term for thermoplastic resins with repeated amide groups on the molecular main chain, including aliphatic, aromatic, and aromatic polyamide fibers [1]. High-strength polyamide fibers are produced through polymerization reactions, usually synthesized from monomers such as caprolactam, adipic acid, and hexamethylenediamine. They have high-strength and high-modulus. Its wear resistance is 10 times higher than cotton and 20 times higher than wool. Adding polyamide fibers to blended fabrics can greatly improve its wear resistance [2, 3]. Polyamide fiber has various applications in industries such as clothing, industry, home furnishings, and packaging materials. Affected by high-strength, wear resistance, corrosion resistance, and ease of processing, polyamide fiber has been widely used in many fields. However, polyamide fibers also have their limitations, such as being easily deformed at high-temperatures and not as breathable as some natural fibers. Therefore, suitable materials need to be selected according to specific application scenarios during usage. When polyamide fiber is stretched to 3%-6%, its elastic recovery rate was 100%. It can withstand multiple bends without breaking, making it an ideal choice for high-performance application materials such as tire curtains, fishing nets, parachute fabrics, etc. [4]. Due to its excellent mechanical properties and chemical resistance, it is extensively applied in textile, au-

tomotive, aerospace, etc. Traditional polyamide fibers are difficult to degrade in natural environments, leading to serious white pollution [5, 6]. The application of titanium dioxide as a photocatalytic material in polymer modification has received widespread attention. Its surface hydroxyl or organic modification can enhance the interfacial bonding with the polymer matrix, thereby improving the photostability and controllable degradation of the material. The synergistic use of titanium dioxide and biodegradable additives can utilize the interface enhancement effect of titanium dioxide to alleviate the phase separation of additives, while optimizing the degradation efficiency through the coupling effect of photocatalysis and biodegradation. The formula design of composite modified titanium dioxide and biodegradable additives used in the study partially refers to the research basis of existing single modification systems. The biodegradable additives are based on the dispersion mechanism of polylactic acid/polyester additives in hydrophobic polymers.

The main contribution of the research is to provide a replicable process paradigm for the development of "high-strength biodegradable" polyamide fibers, which is expected to reduce white pollution in textile, packaging, and other fields, transforming the materials industry towards green manufacturing. Meanwhile, the composite modification strategy has important reference value for expanding the application scenarios of polyamide in harsh environments.

2. Related works

The process optimization of polyamide fibers can improve fiber performance and meet diverse application needs. Van Cong D et al. investigated the possibility of preparing biocomposites from jute fibers and polyamide 11 by modifying the fibers through two methods: alkali treatment and SiO_2 nanoparticle deposition. The modification greatly improved the thermal and mechanical stability of jute fibers. The SiO_2 nanoparticle improved the interaction and adhesion of the fiber matrix [7]. Abdallah S et al. took grey relational analysis to decide the optimal printing parameters based on the polyamide 12 material to explore the influence of input parameters on printed parts. When the strain rate was 10 mm/min and the building orientation was 25°, the optimized grey correlation degree increased by 0.141% [8].

Chen J et al. used aramid fiber filled polyamide 12 for multi-jet melting to improve printed components, to address the limited selection of commercial composite powders for multi-jet melting. The results indicated that the mechanical properties of AF/PA12 composite parts were significantly optimized in the roll coating direction where fibers tended to be arranged [9]. Mishra P K et al. established a finite element model to predict the impact strength and tensile strength of 3D printed polyamide specimens to analyze the layer thickness. When the layer thickness was 0.1 mm and the filling density was 100%, larger interlayer bonding and fewer voids resulted in higher tensile and bending strength [10]. Khalid N N et al. found a mechanism to achieve good interface adhesion mainly through dry printed samples to solve the interface adhesion in the lack of stacked sequences in melt deposition modeling, and form appropriate adhesion on the layers. The results showed that compared with pure polyamide, the bending strength increased by 23% and the impact strength increased by 240% [11].

The research on polyamide fiber modification mainly focuses on single factor optimization or specific process improvement. Existing studies mostly focus on improving mechanical properties or single degradation mechanisms, with insufficient attention paid to the synergistic optimization of biodegradability and mechanical properties. There are few systematic studies involving composite modifiers. In addition, the trade-off between degradation efficiency and material properties is not yet clear, and the impact mechanism of environmental factors on degradation behavior still needs to be further explored. Therefore, to enhance the application range of high-strength polyamide fibers and reduce the environmental pollution of such materials, the research optimizes the production process of high-strength polyamide fibers using titanium dioxide, while adding biological additives to improve the biodegradability.

The innovation lies in optimizing the production process of high-strength polyamide fibers using titanium dioxide modification and biodegradable additives. In theory, titanium dioxide modification can affect the optical properties of high-strength polyamide fibers and enhance their full dull performance. Biodegradable additives can degrade high-strength polyamide fibers in natural fibers, reducing the environmental pollution caused by high-strength polyamide fibers.

3. Methods and materials

3.1. Experimental materials and equipment

The main materials include composite modified titanium dioxide, deionized water, caprolactam, etc. The main experimental equipment includes a polymerization kettle, a melt spinning machine, a drying oven, etc, as shown in Table 1 [12, 13].

Table 1. Galaxy information of experimental raw materials and equipment.

Name	Type	Name	Type
Composite modified titanium dioxide	\	High-shear dispersing emulsifier	FA25
Deionized water	\	Caprolactam	Technically pure
Adipic acid	Analytical pure	Pelletizer	JD1A-40
PVC	GSHA-5L	DHG	DHG-9030A
Melt Spinning System	ABEφ25X5	Parallel stretching machine	TF-100
Drum dryer	SZG-100	Analytical balance	ME204E/02
Induction cooker	C21-WK2102	Vacuum oven	DZF
Electronic fabric strength tester	HD026N	Fully automatic surface area and porosity analyzer	QP-2010Ultra

3.2. Production process of high-strength polyamide fiber

Emulsification and in-situ polymerization of high-strength polyamide slices: Firstly, weigh caprolactam and heat it to melt [14, 15]. Secondly, mix liquid caprolactam with modified titanium dioxide and biodegradable additives, and use a high-shear dispersing emulsifier for emulsification and dispersion to uniformly distribute titanium dioxide and biodegradable additives in caprolactam [16, 17]. Thirdly, add the emulsified and dispersed solution along with the remaining caprolactam into the polymerization reactor. Fourthly, under nitrogen protection, raise the temperature inside the kettle to 255-258°C, maintain the pressure, and carry out the hydrolysis and ring opening reaction. Fifthly, amide polymerization: After pressure relief, continue to introduce nitrogen gas, adjust the stirring speed to control the polymerization, and carry out amide polymerization reaction. Sixthly, after the vacuum reaction, inject nitrogen gas to increase the pressure, discharge the material, and solidify in a water tank before being cut into pellets. Seventhly, extract the polymerized slices with deionized water at $90-100$°C for 24 hours, and replace the water every 3 hours. Eighthly, dry the extracted slices in a drum at 130°C for 48 hours to remove moisture and prepare for melting [18, 19]. Ninthly, melt the slices at 270°C and prepare for spinning. Tenthly, press out the melted slices through the nozzle, perform oiling, pre-stretching, and winding. Next, stretch the fibers at 250 m/min to achieve the desired fineness and strength.

When preparing experimental materials, five different samples were prepared by adjusting the content of composite modified titanium dioxide and biodegradable additives. The content of composite modified titanium dioxide and biodegradable additives in sample 1 is 0%. The content of composite modified titanium dioxide and biodegradable additives in sample 2 is 0% and 1%, respectively. The content of composite modified titanium dioxide and biodegradable additives in sample 3 is 0% and 2%, respectively. The content of composite modified titanium dioxide and biodegradable additives in sample 4 is 1%. The content of composite modified titanium dioxide and biodegradable additives in sample 5 is 1% and 2%, respectively.

3.3. Test method

The biodegradation testing method adopts soil landfill method. The soil at a depth of 20cm from the ground is collected as experimental landfill material. The soil moisture should be maintained between 45% and 50%, and the soil pH should be kept around 7.0 [20, 21]. The initially collected soil needs to be screened before it can be used directly. A 0.25cm diameter sieve is used to screen the soil sample and remove substances such as fallen leaves and stones. The species samples prepared in the experiment are buried in soil samples for degradation treatment.

After the experimental material degrades for a period of time, the sample is taken out, washed and dried, and the sample is weighed by adding wet weight. The above steps are performed once every 25 days for 5 times. The weight loss of the sample is displayed in Eq. (1).

$$a = \frac{m_0 - m_i}{m_0} \times 100\% \tag{1}$$

In Eq. (1), a represents the weight loss. m_0 represents the initial weight of the experimental sample. m_i represents the quality of the i-th sample test. The mechanical properties of the experimental samples are tested using a parallel stretching machine with a stretching speed of 100 mm/min and a pre-tension of 2 N . The experimental samples were subjected to thermogravimetric analysis using a thermogravimetric analyzer. After placing the experimental sample in the crucible, the thermogravimetric analyzer is used for testing. The testing temperature ranges from 45°C to 700°C. The protective gas during the thermogravimetric process is nitrogen, with a temperature rise gradient of 20°C/min [22, 23]. The experiment is repeated five times, and the mean value is obtained after removing

the abnormal values to reduce the influence of accidental factors on the experimental results.

After degrading the experimental sample, SEM testing is also required. After 62 and 125 days of soil degradation treatment, the experimental samples are taken out, washed, dried, and subjected to gold spraying treatment. The morphological changes of the processed sample after soil degradation are observed [24, 25]. The changes in the macromolecular chain structure in the sample material can also reflect the biodegradation of the sample. The study analyzes the macromolecular structure of the sample. The changes in the structure of macromolecules are tested using gas chromatography, and the gas chromatograph used in the experiment is a flame ionization detector. The specific operating steps are described in the instruction manual [26]. The experiment is repeated five times and the mean is taken after removing the outliers.

4. Results and discussion

4.1. Thermogravimetric analysis and degradation quality loss results of experimental samples

The study conducted thermal weight loss and soil degradation quality loss detection on the experimental samples, as presented in Fig. 1. Fig. 1 (a) displays the change in soil degradation quality. With the continuous increase of soil degradation treatment time, the residual mass of experimental samples 2 and 3 continued to decrease, and the decrease rate also continued to increase. After 125 days of soil degradation, the residual mass of experimental sample 2 was 4.46 g . After 125 days, the participating mass of experimental sample 3 was 4.34 g . The quality loss rate of experimental sample 2 was approximately 8.413%. The quality loss rate of experimental sample 3 was approximately 11.796%. The soil degradation effect of sample 4 was basically consistent with that of sample 2, and the soil degradation effect of sample 5 was basically consistent with the sudden degradation effect of sample 3. The experimental results indicated that modified titanium dioxide had a relatively small impact on the soil degradation effect of the material. Fig. 1(b) displays the thermogravimetric analysis of the experimental sample. The temperature at which the experimental sample began to decompose was 400°C, and complete decomposition occurred at 650°C. In thermogravimetric analysis, the residual mass of sample 1 was 0.046%, the sample 2 was 1.989%, the sample 3 was 1.762%, the sample 4 was 3.012%%, and the sample 5 was 2.845%. The main components of biodegradable additives are organic molecular structures, which are easily decomposed by soil microorganisms. After decomposing the biological additive, the structure of polyamide fibers is destroyed, and some structures detach from the sample, resulting in an accelerated biodegradation rate.

4.2. Mechanical performance test results of experimental samples

The study tested the fracture strength and mechanical performance of different samples, as presented in Fig. 2. Fig. 2(a) displays the changes in the fracture strength after adding biodegradable additives. In sample 1, no biodegradable additives were added, and the fracture strength remained at around 205N. In sample 2, 1% of biodegradable additives were added, and the fracture strength of the sample remained around 195N throughout the testing. In sample 3, 2% of biodegradable additives were added, and the fracture strength remained around 110N throughout the testing. As the content of additives increased, the fracture strength of the experimental samples gradually decreased. The fracture strength of sample 4 showed that its fracture strength was slightly higher than that of sample 2. Meanwhile, the fracture strength of sample 5 was much higher than that of sample 5. The study suggests that the composite modified titanium dioxide improves the damage of biodegradable additives to the material structure to a certain extent and enhances the fracture strength of the sample. Fig. 2(b) displays the mechanical performance curves of different samples. The fiber strength of the experimental sample without adding composite titanium dioxide reached 4.2, which was about 0.55 times higher than that of the experimental sample modified with composite titanium dioxide. The titanium dioxide can be considered as a defect in the fibers, leading to stress concentration and easy fracture inside the fibers, and resulting in a decrease in strength within the normal range.

The study further tested the effect of biodegradable additives on the fracture elongation and fracture energy of the samples, as displayed in Fig. 3. Fig. 3(a) displays the effect of the content of biological additives on the fracture elongation. With the increase of additive content, the average elongation at break decreased from 149.2mm to 132.4mm, and the highest value could decrease to 121.2mm. The variation coefficient of elongation at break increased from 7.2% to 10.1%, and further increased to 19.2%. Fig. 3(b) displays the effect of biodegradable additives on the fracture energy. The fracture energy of sample 1 remained around 1.7J, and the fracture energy of sample 2 remained around 1.4J. The fracture energy of sample 3 remained around 0.8J. As the amount of biodegradable additives added further increased, the fracture energy of the sample gradually decreased.

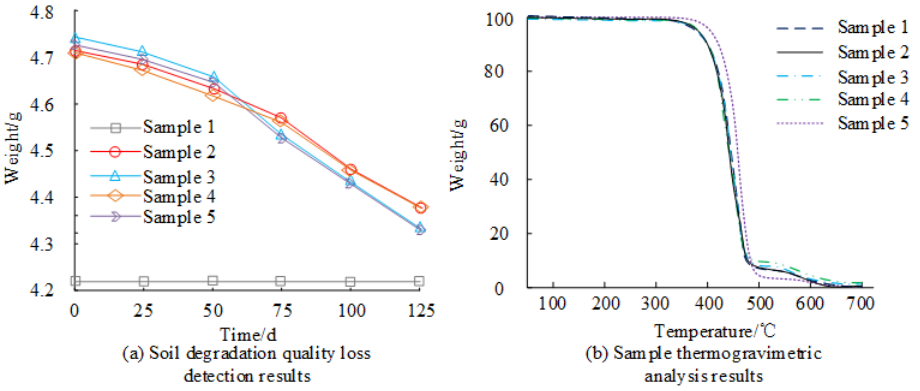

Fig. 1. Results of the degradation quality and thermogravimetric analysis of the experimental samples: (a) Soil degradation quality loss detection results; (b) Sample thermogravimetric analysis results.

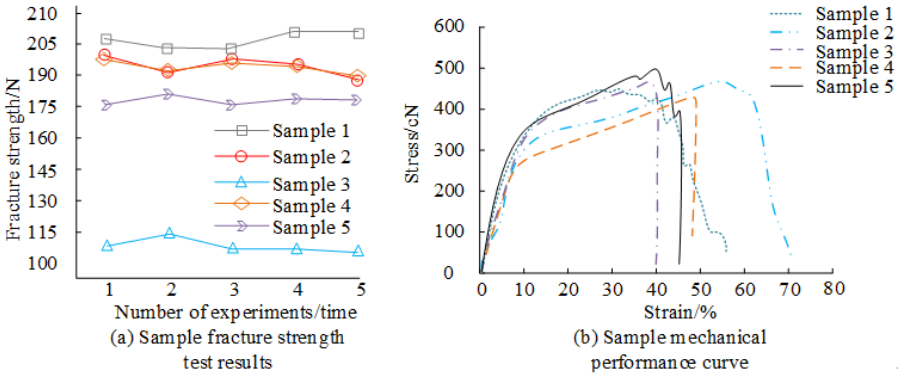

Fig. 2. Mechanical performance curve of fracture force machine in experimental samples: (a) Sample fracture strength test results; (b) Sample mechanical performance curve.

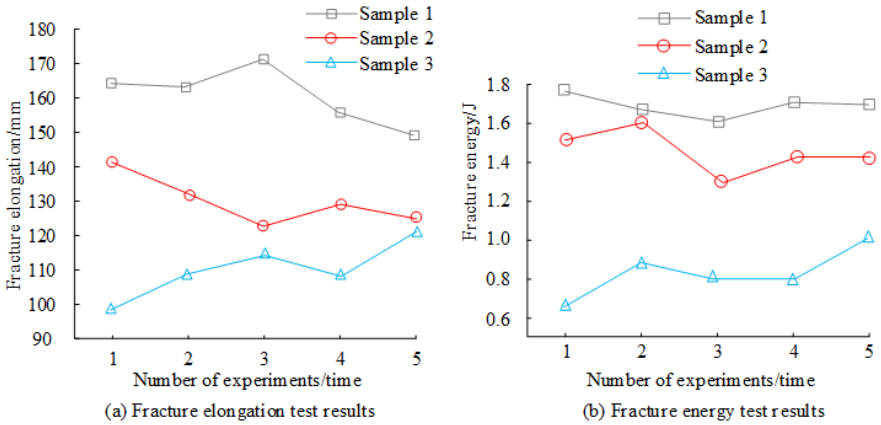

Fig. 3. Sample fracture elongation and fracture energy test results: (a) Fracture elongation test results; (b) Fracture energy test results.

4.3. Microstructure analysis of experimental samples

The microstructure of the sample after adding composite titanium dioxide modifier and biodegradation assistant was analyzed, as presented in Fig. 4. Fig. 4(a) shows the SEM image of sample 2, Figure 4 (b) shows the SEM image of sample 3, Fig. 4(c) shows the SEM image of sample 4, and Fig. 4(d) shows the SEM image of sample 5. The red

circles in Fig. 4(a) and Fig. 4(b) represent the aggregation and pore structure observed in the material structure after adding biodegradable additives. There were obvious agglomerated particles of additives on the surfaces of samples 2 and 3, with a diameter of about $1-3\mu$m and irregular pores of about $0.5-2\mu$m. The pore distribution was uneven, and some areas formed locally connected structures, which became stress concentration points. In samples 4 and 5, the additive and titanium dioxide were uniformly dispersed in the matrix as nanoscale articles, with no significant interfacial separation and a smooth and dense surface. Modified titanium dioxide may enhance interfacial compatibility and inhibit phase separation through physical adsorption or hydrogen bonding between surface functional groups, additives, and polyamide molecular chains. This homogenized structure reduces micro defects, delays the decline in mechanical properties, and provides a more uniform erosion path for microbial degradation, explaining the phenomenon of sample 5 maintaining high structural integrity after 125 days.

The study also tested the microstructure changes of the experimental samples during the soil degradation process, as displayed in Fig. 5. Fig. 5(a) displays the microstructure changes of sample 4 after 0 days of degradation in soil degradation testing, Fig. 5(b) displays the microstructure changes of sample 4 after 62 days of degradation in soil degradation testing, and Fig. 5(c) displays the microstructure changes of sample 4 after 125 days of degradation in soil degradation testing. Before landfilling degradation treatment, the surface structure and fiber morphology of the experimental sample were clear, without wrinkles or fractures. After 62 days, the fiber surface showed peeling phenomenon. After 125 days, the fiber surface showed obvious wrinkling phenomenon, but no obvious fiber fracture phenomenon. According to the thermogravimetric analysis and soil degradation analysis of the samples, adding composite modified titanium dioxide does not affect the biodegradation effect of the sample.

4.4. Experimental sample infrared spectrum results

According to the infrared spectroscopy study of soil degradation, the chemical bond vibration characteristics of sample 1 and sample 5 showed different changes during the degradation process. For sample 1, within the wave number adjustment ($3,292-3,302\ \mathrm{cm}^{-1}$), the single peak of nitrogen hydrogen bond stretching vibration remained stable throughout the degradation period. There was no significant change in the stretching vibration ($2,935-2,946\ \mathrm{cm}^{-1}$) and symmetric stretching vibration ($2,860-2,870\ \mathrm{cm}^{-1}$) of the carbon hydrogen bond. The stretching vibration of carbon oxygen bond (1,629-1,640 cm^{-1}) also showed no significant changes. The peaks generated by the overlap of nitrogen hydrogen bond bending vibration and carbon nitrogen bond stretching vibration $(1,533-1,543\ \mathrm{cm}^{-1}$ and $1,257-1,267\ \mathrm{cm}^{-1})$ remained almost unchanged. In contrast, sample 5 exhibited different characteristics of degradation within the same time span. The stretching vibration of nitrogen hydrogen bonds ($3,293-3,303\ \mathrm{cm}^{-1}$) showed an increase in transmittance during the later stage of degradation, indicating a decrease in the concentration of this component. The stretching vibration of the carbon hydrogen bond $(2,921-2,931\ \mathrm{cm}^{-1})$ resulted in a decrease in transmittance after 125 days, indicating an increase in concentration and a shift in peak position. The symmetric stretching vibration $(2,851-2,861\ \mathrm{cm}^{-1})$ also showed decreased transmittance, increased concentration, and shifted peak position. A slight increase in transmittance was observed during the stretching vibration of carbon oxygen bonds ($1,634-1,645\ \mathrm{cm}^{-1}$), indicating a slight decrease in concentration. The overlapping peaks of nitrogen hydrogen bond bending vibration and carbon nitrogen bond stretching vibration $(1,535-1,545\ \mathrm{cm}^{-1}$ and $1,257-1,268\ \mathrm{cm}^{-1})$ demonstrated no obvious changes during the degradation process, as presented in Fig. 6.

4.5. Changes in macromolecular chains of experimental samples

The macromolecular chains of sample 1 before soil degradation are shown in Table 2. During the high-temperature cracking process, polyamide macromolecules underwent decomposition, with the main decomposition product being caprolactam, which was the monomer component of polyamide. This phenomenon reveals that under high-temperature conditions, the amide bonds in polyamide molecular chains are relatively fragile and prone to breakage. The research shows that the chemical stability of amide bonds is relatively weak, and these bonds are prone to breakage when the environment undergoes drastic changes, especially under high-temperature conditions. Under high-temperature, chemical groups in the structure of polyamide macromolecules may form closed loops, generating caprolactam. In the cracking product, compared with the relative molecular weight of caprolactam, the component with smaller molecular weight accounted for 14.26%, while the component with larger molecular weight accounted for 83.67%. This process not only involves the cleavage of amide bonds, but may also involve irregular cleavage or recombination under high-temperature conditions, with amide bonds and bond connecting the benzene ring to the amide group being the main cleavage points. These breaks

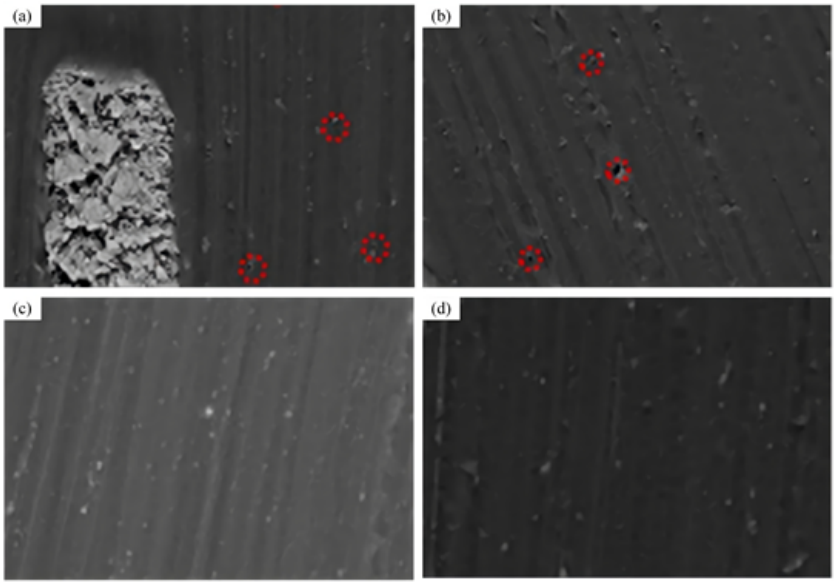

Fig. 4. Microstructure changes during soil degradation in sample 4: (a) displays the microstructure changes of sample 4 after 0 days of degradation in soil degradation testing; (b) displays the microstructure changes of sample 4 after 62 days of degradation in soil degradation testing.

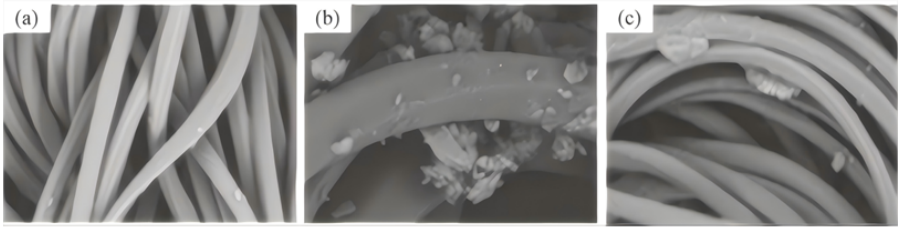

Fig. 5. Microstructure changes during soil degradation in sample 4: (a) displays the microstructure changes of sample 4 after 0 days of degradation in soil degradation testing; (b) displays the microstructure changes of sample 4 after 62 days of degradation in soil degradation testing.

ultimately lead to the formation of small molecules such as caprolactam, as well as the possible enamide substances.

The study further analyzed the rate differences of each sample at different degradation stages. Sample 1 lost only 3.2% in mass from 0-62 days, and the degradation rate stagnated in the later stage due to the lack of active sites. Sample 3 containing 2% additives exhibited non-linear accelerated degradation characteristics, with a loss rate of 12.7% in the first 62 days. In the later stage, due to the dissolution of additives, a porous structure was formed, and microbial infiltration was enhanced, resulting in a monthly growth of 5.9%. Although the total degradation rate of sample 5 was similar to that of sample 3, its degradation process was more uniform. This is attributed to the continuous activation of the auxiliary agent by the micro oxidation environment generated by TiO_2 photocatalysis, which avoids the later efficiency degradation caused by the rapid loss of auxiliary agents in sample 3. The research system synergistically increases the degradation rate to 3.7 times that of traditional materials.

5. Conclusion

To improve the biodegradability of high-strength polyamide fibers and reduce the impact of structural changes on their mechanical properties, the research optimized the production process of high-strength polyamide fibers by combining composite modified titanium dioxide with biodegradable additives. After 125 days of degradation, the weight loss of sample 3 was 18.583%. During the soil landfill degradation process, the degradation rate of the experimental sample gradually increased, indicating that the production process optimization effect was good.

Table 2. Major macromolecular chains before the degradation of sample 1.

Name	Content (%)	Retention time (min)
Alanine	10.14	1.783
Cyclopentanone	2.13	5.467
5-Cyano-1-pentene	1.71	6.820
Hexanenitrile	1.23	7.103
Caprolactam	73.43	13.001
6-Aminocapronitrile	3.81	10.710
Isobutylpropylamine	1.12	15.231
N. N-Hexamethylene dimethylformamide	5.24	18.113
N-Hexyl-Butyramide	1.19	16.537

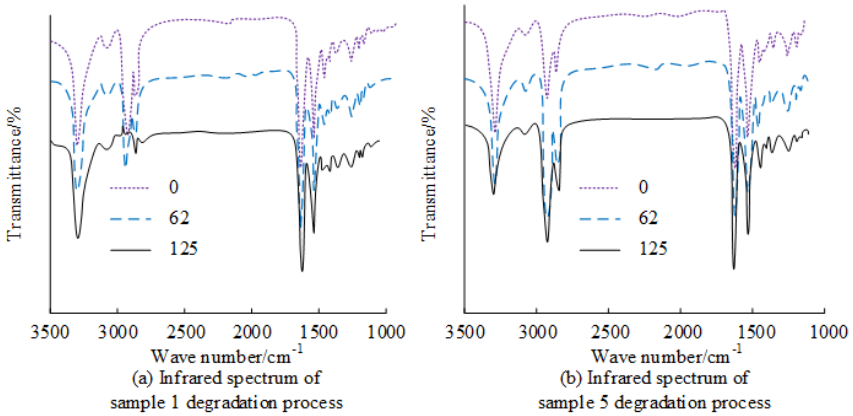

Fig. 6. Infrared spectroscopy results of sample soil degradation: (a) Infrared spectrum of sample 1 degradation process; (b) Infrared spectrum of sample 5 degradation process.

Before landfilling degradation treatment, the surface structure and fiber morphology of the experimental sample were clear, without wrinkles or fractures. After 125 days of degradation, the fiber structure showed significant fracture. In the cracking products, the proportion of components with a relative molecular weight less than that of the macromolecular chain was adjusted to 18.57%, while the proportion of components with a relatively large molecular weight of the macromolecular chain was adjusted to 81.43%. Sample 1 without added additives had the lowest degradation rate, only 8.4% after 125 days, but had the best mechanical properties. The degradation rate of samples 2 and 3 containing only biodegradable additives increased to 11.8% − 18.6%, but the fracture strength decreased by 4.9% and 46.3%, respectively.

Samples 4 and 5 containing 1% composite modified TiO_2 showed a significant reduction in mechanical performance while approaching the degradation rate of sample 3. This indicates that the interface enhancement effect of TiO_2 effectively alleviates the structural defects caused by additives, achieving the optimal balance between degradation efficiency and mechanical stability. The differences in the content of composite titanium dioxide and biodegradable additives in different samples affect the degradation rate and dispersibility. Fluctuations in environmental conditions such as soil moisture and pH may have uneven effects on the degradation process. In addition, the testing interval between 62 days and 125 days may not fully capture the critical points of certain structural changes, and small differences in the sample preparation process may also lead to inconsistent degradation behavior. The specific mechanism is further validated through controlled variable experiments or extended testing periods. At high-temperatures, the chemical groups in the polyamide macromolecule structure form closed loops, producing caprolactam. However, this study reduces the mechanical properties of high-strength polyamide fiber structure when optimizing it. In the future, the research will further analyze the structure of high-strength polyamide fibers, optimizing their biodegradability while ensuring the mechanical properties to further reduce the environmental impact of such materials.

References

[1] K. Głowacka, J. Małecka, and T. Smolnicki, (2024) *"Analysis of the Surface Topography of Fractures Caused*

by Static and Impact Bending of Polypropylene and Polyamide PA6 Reinforced with Continuous Glass Fibers" **Advances in Science & Technology Research Journal *18***(5): 51–64.

[2] W. Wang, M. Peng, Z. Wang, and Y. Liu, *"Fully aminated rigid-rod aromatic polyamide efficiently reinforces tetraglycidyl diamino diphenyl methane epoxy resin and its carbon fiber composite"* **Polymer Composites *45***(6): 5725–5736. DOI: 10.1002/pc.28159.

[3] Y. Duo, X. Qian, B. Zhao, L. Gao, H. Bai, X. Guo, and B. Song, (2022) *"Preparation and properties of fluffy high-shrinkage polyester/polyamide 6 hollow segmented pie microfiber nonwovens"* **Textile Research Journal *92***(17-18): 3221–3233. DOI: 10.1177/00405175211062098.

[4] Z. LIU, Z. SHEN, G. SONG, C. C. andbGegu CHEN, and F. PENG, (2024) *"Preparation and properties of high-strength and waterproofing wood-derived bioplastic"* **Journal of Forestry Engineering *9***(04): 105–111. DOI: 10.13360/j.issn.2096-1359.202309042.

[5] H. Wu, J. Qiu, G. Zhang, E. Sakai, W. Zhao, J. Tang, H. Wu, and S. Guo, *"Distribution and reinforcement effect of carbon fiber at the interface in injection welding of polyamide 6 composites"* **Polymer Composites *45***(2): 1347–1360. DOI: 10.1002/pc.27858.

[6] H. Zhang and W.-f. Sun, (2023) *"Mechanical properties and failure behavior of 3D printed thermoplastic composites using continuous basalt fiber under high-volume fraction"* **Defence Technology *27***: 237–250. DOI: 10.1016/j.dt.2022.07.010.

[7] D. Van Cong, N. V. Giang, T. H. Trung, P. Q. Tuan, N. T. Thai, D. Q. Tham, M. Van Tien, and D. V. Quang, *"Novel biocomposite from polyamide 11 and jute fibres: the significance of fibre modification with SiO2 nanoparticles"* **Polymer International *71***(3): 255–265. DOI: 10.1002/pi.6316.

[8] S. Abdallah, S. Ali, and S. Pervaiz, (2023) *"Performance optimization of 3D printed polyamide 12 via Multi Jet Fusion: A Taguchi grey relational analysis (TGRA)"* **International Journal of Lightweight Materials and Manufacture *6***(1): 72–81. DOI: 10.1016/j.ijlmm.2022.05.004.

[9] J. Chen, P. Tan, X. Liu, W. S. Tey, A. Ong, L. Zhao, and K. Z. and, (2022) *"High-strength light-weight aramid fibre/polyamide 12 composites printed by Multi Jet Fusion"* **Virtual and Physical Prototyping *17***(2): 295–307. DOI: 10.1080/17452759.2022.2036931.

[10] P. K. Mishra, B. Karthik, and T. agadesh, (2024) *"Finite element modelling and experimental investigation of tensile, flexural, and impact behaviour of 3D-printed polyamide"* **Journal of The Institution of Engineers (India): Series D *105***(1): 275–283. DOI: 10.1007/s40033-023-00477-8.

[11] N. N. Khalid, N. A. M. Radzuan, A. B. Sulong, F. M. Foudzi, and D. Hui, *"Adhesion behaviour of 3D printed polyamide–carbon fibre composite filament"* **REVIEWS ON ADVANCED MATERIALS SCIENCE *61***(1): 838–848. DOI: 10.1515/rams-2022-0281.

[12] M. M. Brette, A. H. Holm, A. D. Drozdov, and J. d. C. Christiansen, (2024) *"Pure Hydrolysis of Polyamides: A Comparative Study"* **Chemistry *6***(1): 13–50. DOI: 10.3390/chemistry6010002.

[13] C. Meng and X. Liu, *"Study on thermal degradation kinetics of bio-based semi-aromatic high-temperature polyamide PA5T/56 and the effect of benzene ring"* **Iranian Polymer Journal *31***(5): 641–650. DOI: 10.1007/s13726-021-01018-4.

[14] E. M. Zakharyan and A. L. Maksimov, *"Pyrolysis of polyamide-containing materials. Process features and composition of reaction products"* **Russian Journal of Applied Chemistry *95***(7): 895–928. DOI: 10.1134/S1070427222070011.

[15] Y. An, T. Kajiwara, A. Padermshoke, T. Van Nguyen, S. Feng, H. Mokudai, T. Masaki, M. Takigawa, T. Van Nguyen, H. Masunaga, S. Sasaki, and A. Takahara, (2023) *"Environmental Degradation of Nylon, Poly(ethylene terephthalate) (PET), and Poly(vinylidene fluoride) (PVDF) Fishing Line Fibers"* **ACS Applied Polymer Materials *5***(6): 4427–4436. DOI: 10.1021/acsapm.3c00552.

[16] Y. Shao, Y. Dong, and Y. Yang, (2021) *"Effect of Low-Cycle Fatigue and Hydrothermal Aging on Tensile Properties of Open-Hole Glass Fiber/Polycarbonate and Glass Fiber/Polyamide 6 Composites"* **Fibers and Polymers *22***(9): 2527–2534. DOI: 10.1007/s12221-021-1228-y.

[17] H. Fang, F. Jia, S. Chen, W. Zhang, L. Huang, F. Wu, H. Chen, D. Lin, and J. Jia, *"Significant enhancement of mechanical properties for glass fiber fabric-reinforced polyamide 6 composites by improving interfacial bonding"* **Polymer Composites *45***(8): 7541–7550. DOI: 10.1002/pc.28285.

[18] K. TANAKA, N. MORIOKA, M. KAWAGUCHI, and K. WATANABE, (2022) *"Effect of Silica Addition to Resin on Fiber Matrix Interfacial Shear Strength of Carbon Fiber Reinforced Polyamide Resin at High Temper-*

ature" **Journal of the Society of Materials Science, Japan *71***(6): 501–507. DOI: 10.2472/jsms.71.501.

[19] W. Chen, Z. Hu, X. Li, J. He, S. Wang, Y. Zhao, M. Li, and J. Zhang, *"Additive manufacturing of high-strength polyamide 6 composites reinforced with continuous carbon fiber prepreg"* **Polymer Composites *45***(1): 668–679. DOI: 10.1002/pc.27805.

[20] W. Zhao, J. Qiu, E. Sakai, H. Wu, Y. Zhao, H. Feng, S. Guo, and H. Wu, *"Ultra-high bonding strength of carbon fiber–doped polyamide–aluminum alloy composite structure achieved by changing crystallinity"* **Polymer Composites *45***(14): 13089–13098. DOI: 10.1002/pc.28688.

[21] , (2024) *"Controllable large-scale processing of temperature regulating sheath-core fibers with high-enthalpy for thermal management"* **Nano Materials Science *6***(3): 337–344. DOI: 10.1016/j.nanoms.2023.10.004.

[22] D. Kwon, S.-K. Park, and Y. Yoo, (2024) *"Flow enhanced high-filled polyamide composites without the strength-flowability trade-off"* **Polymer Bulletin *304***: 14823–14836. DOI: 10.1016/j.apenergy.2021.117766.

[23] M. K. Zeybek, M. Güden, and A. Taşdemirci, (2023) *"The Effect of Strain Rate on the Compression Behavior of Additively Manufactured Short Carbon Fiber-Reinforced Polyamide Composites with Different Layer Heights, Infill Patterns, and Built Angles"* **Journal of Materials Engineering and Performance *32***: 11050–11063. DOI: 10.1007/s11665-023-07918-1.

[24] X. Zhai, J. Chen, R. Su, X. Gao, X. Zhang, and R. He, *"Vat photopolymerization 3D printing of Al2O3 ceramic cores with strip-shaped pores by using polyamide 6 fiber template"* **Journal of the American Ceramic Society *107***(8): 5400–5411. DOI: 10.1111/jace.19836.

[25] J. Wang, S. Yu, J. Zhou, C. Liang, W. Huang, Z. Hu, Z. Chen, H. Xiang, and M. Zhu, *"Discrete molecular weight strategy modulates hydrogen bonding-induced crystallization and chain orientation for melt-spun high-strength polyamide fibers"* **Polymer Engineering & Science *64***(9): 4053–4063. DOI: 10.1002/pen.26832.

[26] L. Mészáros, Á. Bezerédi, and R. Petrény, *"Modifying the properties of polyamide 6 with high-performance environmentally friendly nano- and microsized reinforcing materials"* **Polymer Composites *45***(7): 6404–6413. DOI: 10.1002/pc.28205.